Appl Phys B (2010) 98: 773–778
DOI 10.1007/s00340-009-3810-7

Applied Physics B
Lasers and Optics

Low threshold current density, low resistance oxide-confined VCSEL fabricated by a dielectric-free approach

Y. Ding · W.J. Fan · D.W. Xu · C.Z. Tong · Y. Liu · L.J. Zhao

Received: 30 June 2009 / Revised version: 14 October 2009 / Published online: 7 November 2009

Abstract We present the fabrication process and experimental results of 850-nm oxide-confined vertical cavity surface emitting lasers (VCSELs) fabricated by using dielectric-free approach. The threshold current of 0.4 mA, which corresponds to the threshold current density of 0.5 kA/cm^2, differential resistance of 76 Ω, and maximum output power of more than 5 mW are achieved for the dielectric-free VCSEL with a square oxide aperture size of 9 μm at room temperature (RT). *L–I–V* characteristics of the dielectric-free VCSEL are compared with those of conventional VCSEL with the similar aperture size, which indicates the way to realize low-cost, low-power consumption VCSELs with extremely simple process. Preliminary study of the temperature-dependent *L–I* characteristics and modulation response of the dielectric-free VCSEL are also presented.

PACS 42.55.Px · 85.60.Bt · 85.35.Be

Y. Ding (✉) · W.J. Fan · D.W. Xu · C.Z. Tong
School of Electrical and Electronic Engineering, Nanyang Technological University, Singapore 639798, Republic of Singapore
e-mail: yding@ntu.edu.sg
Fax: +65-67920415

W.J. Fan
e-mail: ewjfan@ntu.edu.sg

Y. Liu
Optoelectronics R&D Center, Institute of Semiconductors, Chinese Academy of Sciences, P.O. Box 912, Beijing 100083, China

L.J. Zhao
Key Laboratory of Semiconductor Materials Science, Institute of Semiconductors, Chinese Academy of Sciences, P.O. Box 912, Beijing 100083, China

1 Introduction

Vertical cavity surface emitting lasers (VCSELs) are attractive light sources for applications in local area networks (LANs), optical interconnects, free-space optical communications, optical data storage, sensors, etc., owing to low-threshold current, circular and low divergence output beams, testability at the wafer level, addressable two-dimensional array integration, and so on. In particular, ultra-low-threshold VCSELs with cost-effective fabrication are expected to be used for compact transmitters [1] or telecom devices containing a large number of transmitters. In these devices, minimized power consumption and low manufacturing cost are needed. For the VCSELs applications besides communications, such as printing, position sensing, etc., low threshold current, low resistance, and lowest process complexity also are desirable in the same way.

A simple fabrication process leads to low manufacturing cost and good reproducibility [2–4]. Generally, dielectric materials including silicon compound (e.g., SiO_2 and SiN_x) or polymer (e.g., polyimide, benzocyclobutene (BCB)), etc., are used for forming electrical isolation layer during the fabrication process of conventional VCSELs [2, 5–7]. Both processing of dielectric materials formation such as SiN_x film deposition or BCB spin coating and the subsequent contact and light output window opening on the dielectric materials increase the production cost and introduce potentially adverse factors for devices' reliability [2]. In well-established oxide-confined VCSELs, an oxidized AlAs or high-Al-content $Al_xGa_{1-x}As$ layer inserted into the top and/or bottom distributed Bragg reflectors (DBRs) produces a current and optical confinement structure [8–11]. In this paper, self-insulation method, i.e., utilizing oxidation layer formed by AlAs or high-Al-content $Al_xGa_{1-x}As$ layer oxidization as electrical isolation layer is brought up to furthest

facilitate the fabrication process. Accordingly, an extremely simple and low-cost fabrication for VCSELs with good features can be achieved. To the best of our knowledge, the dielectric-free VCSEL has the simplest VCSEL fabrication process by far and will be applicable for various active region materials and wavelength. Furthermore, the dielectric-free approach will be promising to realize flexible process for photonic crystal (PhC) VCSELs based on the similar oxidation procedure.

The low threshold current of 0.4 mA, which corresponds to the threshold current density of 0.5 kA/cm^2, differential resistance of 76 Ω, threshold voltage of 1.55 V, and saturated output power of more than 5 mW are achieved for the 850-nm dielectric-free VCSEL with 9-μm size aperture at room temperature. From the comparison of L–I–V characteristics between dielectric-free VCSEL and dielectric-dependent VCSEL, finer optical output features and smaller differential resistance can be obtained for the former. We also preliminarily investigate the temperature-dependent L–I characteristics and modulation response of dielectric-free VCSEL. The modulation bandwidth of over 5 GHz is obtained for the 9-μm oxide aperture dielectric-free VCSEL at bias current of 5 mA without dynamic characteristics optimization. From the transfer function fitting, the improvement of modulation bandwidth can be expected through reducing parasitics in the present devices.

2 Device structure and fabrication process

The VCSEL epitaxial wafers were prepared by metal-organic vapor-phase epitaxy (MOVPE) growth on n$^+$-GaAs substrates. The epitaxial structure consists of a GaAs/$Al_{0.3}Ga_{0.7}As$ multiple quantum-well (MQW) active region between top and bottom distributed Bragg reflector (DBR) mirrors. DBR stacks consist of 21 pairs of p-doped top and 34.5 pairs of n-doped bottom DBR mirrors. Both top and bottom DBR are composed of alternating $Al_{0.9}Ga_{0.1}As$ and $Al_{0.12}Ga_{0.88}As$ layers. Graded interfaces and modulation doping are used to reduce the DBR resistance. Carbon and silicon are used for p-type and n-type dopants, respectively, for the whole structure. A 30-nm-thick $Al_{0.98}Ga_{0.02}As$ layer embedded in p-DBR adjacent to the active region is used for selective wet oxidation.

The fabrication procedures are as follows. First, mesas were formed by lithography and unselective wet-etching as shown in Fig. 1. The solution used for the wet-etching is H_3PO_4:H_2O_2:H_2O = 3:3:10. Mesa includes three parts:

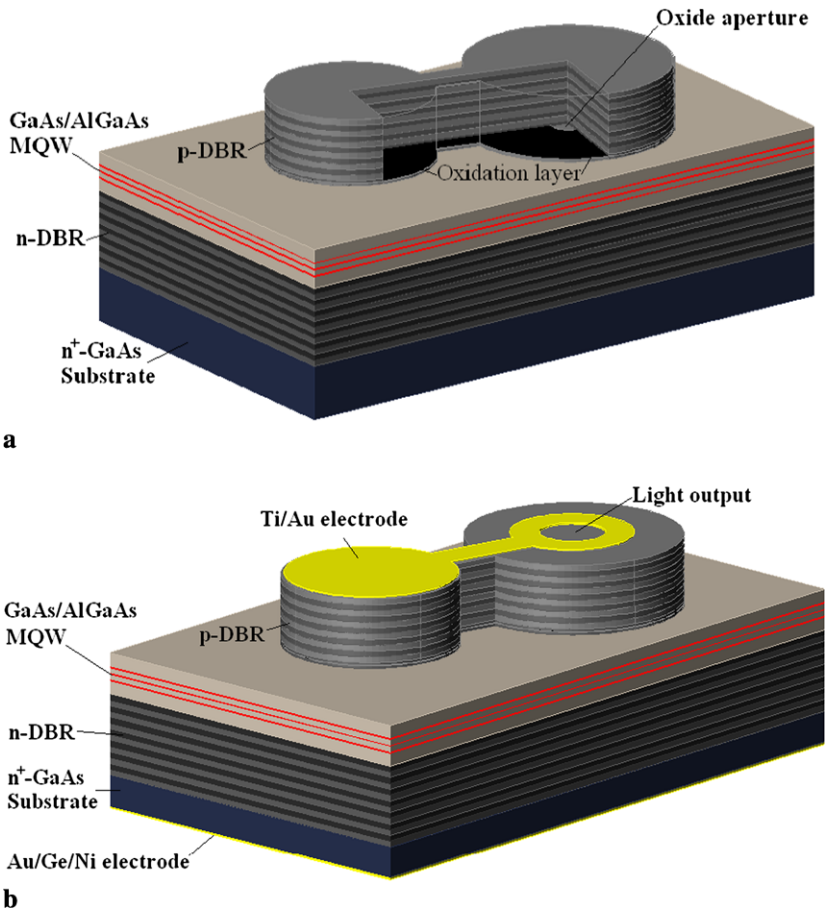

Fig. 1 (**a**) Schematic partial perspective of mesa after wet-etching and followed by $Al_{0.98}Ga_{0.02}As$ oxidization. (**b**) Schematic illustration of a final dielectric-free VCSEL device

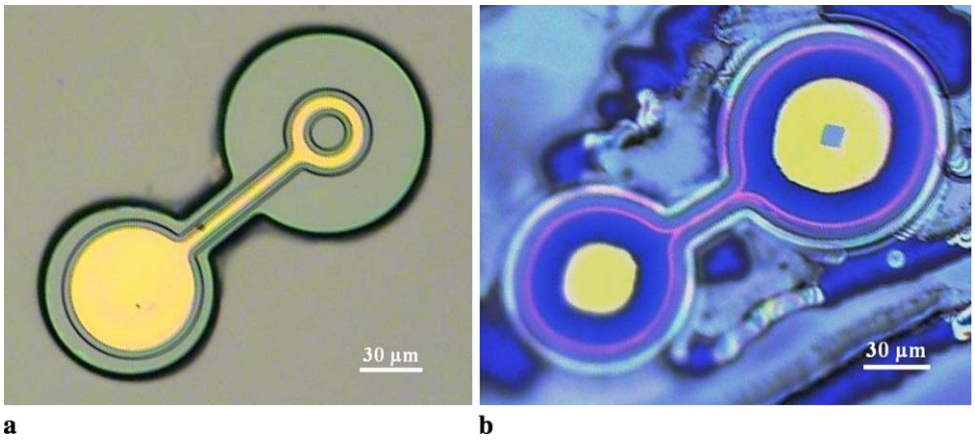

Fig. 2 Microscopic images from top view: (**a**) a final dielectric-free VCSEL device; (**b**) a sample after $Al_{0.98}Ga_{0.02}As$ layer oxidization and removing top DBR stacks

the big circular portion with a diameter varied from 105 to 115 μm is lasers' main body, relatively small circular portion with a diameter of about 90 μm is used for bond pad mesa, and a bridge is used to connect these two portions and to form a conjunct plane. Then, two square oxide apertures of 9 μm and 17 μm in side length were formed by wet oxidization in the lasers' main body circular portion (Fig. 1(a)) with oxidization condition of at 430°C under 1 L/min N_2 gas bubbled through 90°C deionized water. The reason for forming square oxide aperture is due to the oxidization anisotropy in the present epitaxial structure. The size of oxide aperture should be smaller than the difference of the two circular portions, so that self-insulation parts formed by $Al_{0.98}Ga_{0.02}As$ layer oxidization can be fully built after oxidization process and no leakage current existing under the wire bonding area or bridge connector during the device operation.

After oxidization, the p-type contact metal (Ti/Au) was deposited directly on the upper side of the wafer. Then the annular p-contact electrode, electrode bridge connector, and circular bond pad were formed by lithography and removing unwanted Ti/Au (Fig. 1(b)). Finally, the n-type contact metal (Au/Ge/Ni) was deposited on to the bottom side of the wafer after substrate thinning, and conventional metal electrodes annealing was carried out (Fig. 1(b)). The main process only includes two times photolithography, one time oxidization, and one time unselective wet-etching, without other process such as dry-etching, SiN_x film deposition, polymer spin coating, contact and light output window opening, etc. The simplicity of whole fabrication process can even be comparable with that of conventional edge emitting laser. The schematic structure of final VCSEL device is shown in Fig. 1(b). Microscopic images from top view of a final dielectric-free VCSEL device is shown in Fig. 2(a), and Fig. 2(b) shows a sample after $Al_{0.98}Ga_{0.02}As$ layer oxidization and removing top DBR stacks during the fabrication process. A clear square oxide aperture as a color of light cyan can be seen at the center of the lasers' main body.

After VCSEL fabrication, the separated device chips were cleaved and mounted on the heatsinks. Static characteristics under continuous-wave (CW) operation of VCSEL devices were tested by a Keithley lasers L–I–V test system. The small signal response were measured by using a calibrated vector network analyzer (Agilent 8720D, 50-MHz–20-GHz) combined with a 50-μm multimode optical fiber coupling and connected to a high-speed O/E converter (HP 11982A, dc–15-GHz).

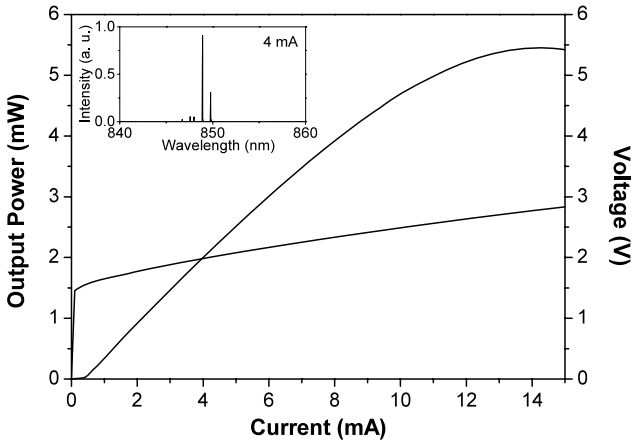

Fig. 3 L–I–V characteristics of dielectric-free VCSEL with oxide aperture size of 9 μm measured at RT. *Inset* is the lasing spectrum at an injection current of 4 mA. The lasing wavelength is 850 nm

3 Results and discussion

Figure 3 shows the measured CW L–I–V characteristic curves for a typical 9-μm side-length aperture dielectric-free VCSEL device at RT. The inset of Fig. 3 is the device's optical spectrum at injection current of 4 mA, where it is seen that the large oxide aperture leads to multimode operation and the center wavelength is at 850 nm. The low threshold current of 0.4 mA, which corresponds to the threshold current density of 0.5 kA/cm^2, is achieved. The threshold power is only 0.62 mW accordingly. This threshold level

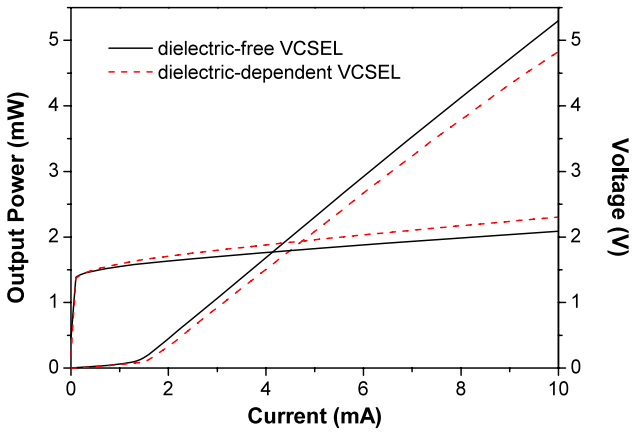

Fig. 4 *L–I–V* characteristics of VCSELs with oxide aperture size of 17 μm. *Solid lines* denote dielectric-free VCSEL and *dashed lines* correspond to dielectric-dependent VCSEL as a reference

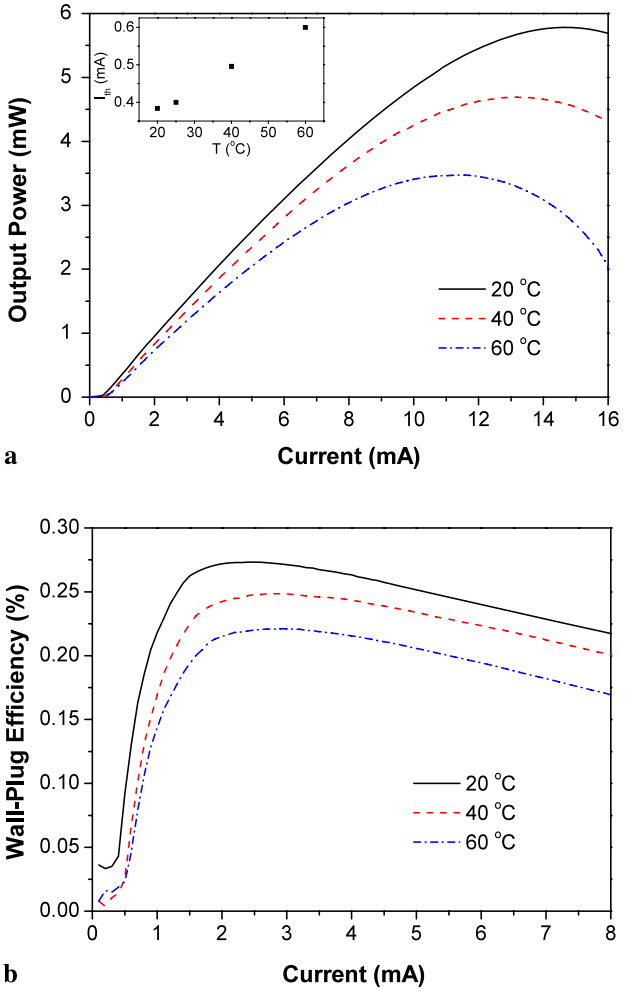

Fig. 5 (**a**) *L–I* characteristics curves; (**b**) wall-plug efficiency curves for 9-μm oxide aperture size dielectric-free VCSEL measured at different temperatures. *Inset* in (**a**) shows the influence of temperature on the threshold current

stands comparison with the forepassed or updated reports of low threshold 850-nm oxide-confined VCSELs fabricated by dielectric-dependent approach [6, 12–16]. The threshold voltage is 1.55 V, only about 90 meV larger than quasi-Fermi level separation. The saturated output power is 5.5 mW at the injection current of 14 mA, and the differential resistance is only 76 Ω and 58 Ω at 10 mA and 15 mA, respectively. The low differential resistance is believed to be due to the large area ohmic contact on the bond pad along with consequently formed much lower p-DBR resistance as shown in Figs. 1(b) and 2(a). It should be noted that since no dielectric materials are used in this device so far, the possibly continued process containing dielectric materials as an etching mask will be easy, such as making photonic crystal deep holes. The often used proton-implantation for reducing the parasitic capacitance is also facile because of a lack of insulator that may induce proton scattering.

The *L–I–V* characteristics comparison at RT between dielectric-free VCSEL and dielectric-dependent VCSEL based on the same epitaxy wafer and with the similar square oxide aperture size of around 17 μm is shown in Fig. 4. Herein, dielectric-dependent VCSEL is fabricated by conventional process with SiN_x film as dielectric material and electrical isolation layer, the details of the fabrication process of which were fully described in our previous report [4]. Both structures are extra-cavity contact with up and down electrodes. The threshold current of 1.42 mA for dielectric-free VCSEL is slightly lower than that of 1.49 mA for dielectric-dependent VCSEL. Correspondingly, the threshold power of dielectric-free VCSEL is about 9 percent lower than that of dielectric-dependent VCSEL. In addition, at an injection current of 10 mA, the differential resistance of dielectric-free VCSEL (49 Ω) is also lower than that of dielectric-dependent VCSEL (64 Ω). From threshold current to 10 mA, both of the output power characteristics curves are linear with slope efficiencies approximately 0.63 W/A and 0.58 W/A, respectively. The lower differential resistance and higher slope efficiency in the dielectric-free VCSEL device can be attributed to a much lower ohmic contact resistance, large area current channel in the p-DBR above oxide layer corresponds to less Joule heating, and simple process corresponds to less failing and, what is more important, is to lead to the lower threshold current.

The *L–I* characteristics of dielectric-free VCSEL with 9-μm oxide aperture size measured at different temperatures are shown in Fig. 5(a). Inset of Fig. 5(a) is the relation between threshold current I_{th} and temperature T. The low threshold current of only 384 μA, which corresponds to the threshold current density of 480 A/cm^2, can be seen at the test temperature of 20°C. The threshold current increases to 0.6 mA as the temperature increases to 60°C. The characteristic curves above 60°C are not measured due to limitation of the measurement equipment. From the trend of temperature increase from 20°C to 60°C, ultra-low threshold current

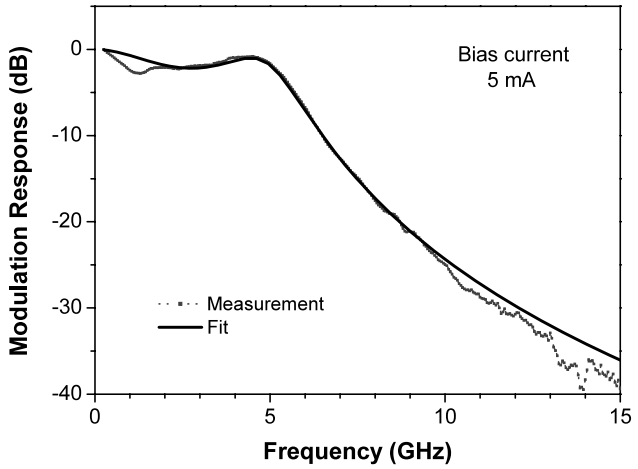

Fig. 6 Small signal modulation response of 9-μm oxide aperture size dielectric-free VCSEL at 5 mA (*dot line*). The *solid line* is fitting to the modulation response based on (1)

density (not more than 0.75 kA/cm^2) and acceptable temperature stability in the threshold current as well as slope efficiency can be obtained. Figure 5(b) shows that the peak wall-plug efficiency is 27.35% at 20°C, and over 22% at 60°C it indicates the acceptable power conversion.

Figure 6 shows the measured small signal frequency response (S_{21}) of the dielectric-free VCSEL with 9-μm oxide aperture size under bias current of 5 mA at RT. As seen in Fig. 6, the response curve drops down quickly with the increased modulation frequency and cut off at around 5.2 GHz. However, the 3-dB bandwidth of a referenced dielectric-dependent VCSEL is 6.9 GHz at 4 mA, 8.1 GHz at 6 mA, and 10 GHz at 10 mA (not shown here), which is obviously wider than that of dielectric-free VCSEL.

The three-pole transfer function [4]

$$H(f) = const \cdot \frac{f_r^2}{(f_r^2 - f^2 + j\frac{f}{2\pi}\gamma)} \cdot \frac{1}{(1 + j(\frac{f}{f_p}))} \qquad (1)$$

was used for fitting to the measured modulation response in order to deduce the basic dynamic parameters, where f_r is resonance frequency, γ is damping factor, and f_p is parasitic cutoff frequency. The resonance frequency f_r of 5 GHz, parasitic cutoff f_p of 2 GHz and γ of 14 GHz can be obtained for the above-mentioned dielectric-free VCSEL, which hints the 3-dB modulation bandwidth restricted at ∼5.2 GHz owing to the external parasitics cut-off. The parasitics should be mainly from the parasitic capacitance of the pad and large area current distribution, which can be decreased by optimizing the mesa's morphology design or introducing proton implantation [13, 14] for the present devices. Further optimization will be carried out to improve the devices' modulation characteristics.

4 Conclusions

We set forth the fabrication process and experimental results of 850-nm oxide-confined VCSELs with a dielectric-free approach. The threshold current density of 0.5 kA/cm^2 is achieved for the dielectric-free VCSEL with a square active region size of 9 μm at room temperature (RT). The VCSEL devices exhibit very low differential resistance within the operation range. Comparison of L–I–V characteristics between dielectric-free VCSEL and dielectric-dependent VCSEL fabricated based on the same epitaxy structure and with the similar aperture size indicates the way to realize low-cost, low-power consumption oxide-confined VCSELs. Preliminary study of the temperature-dependent L–I characteristics and modulation response of dielectric-free VCSEL are also presented, and the corresponding results are discussed. This approach will be promising for commercial production of oxide-confined VCSELs and PhC VCSELs fabrication with various active region materials and wavelength.

Acknowledgements The authors acknowledge the financial support from the A*STAR Singapore–Poland Bilateral Program, SERC Grant No. 0621200015. The authors would like to thank Associate Professor L.F. Wang and Ms. J. Bian of Chinese Academy of Sciences for their technical support.

References

1. J. Park, T. Kim, S.H. Kim, S.B. Kim, Opt. Express **7**, 5147 (2009)
2. H.C. Yu, S.J. Chang, Y.K. Su, C.P. Sung, Y.W. Lin, H.P. Yang, C.Y. Huang, J.M. Wang, Mater. Sci. Eng. B, Solid State Mater. Adv. Technol. **106**, 101 (2004)
3. Y. Ding, W.J. Fan, D.W. Xu, C.Z. Tong, W.K. Loke, S.F. Yoon, D.H. Zhang, Y. Liu, N.H. Zhu, L.J. Zhao, W. Wang, Proc. SPIE **7158**, 715807 (2008)
4. Y. Ding, W.J. Fan, D.W. Xu, C.Z. Tong, S.F. Yoon, D.H. Zhang, L.J. Zhao, W. Wang, Y. Liu, N.H. Zhu, J. Phys. D, Appl. Phys. **42**, 085117 (2009)
5. A.N. AL-Omari, G.P. Garey, S. Hallstein, J.P. Watson, G. Dang, K.L. Lear, IEEE Photonics Technol. Lett **18**, 1225 (2006)
6. P. Westbergh, J.S. Gustavsson, A. Haglund, H. Sunnerud, A. Larsson, Electron. Lett. **44**, 907 (2008)
7. Y. Sugawara, T. Miyamoto, Electron. Lett. **45**, 167 (2009)
8. B. Weigl, M. Grabherr, C. Jung, R. Jager, G. Reiner, R. Michalzik, D. Sowada, K.J. Ebeling, IEEE J. Sel. Top. Quantum Electron. **3**, 409 (1997)
9. W. Nakwaski, M. Wasiak, P. Mackowiak, W. Bedyk, M. Osinski, A. Passaseo, V. Tasco, M.T. Todaro, M. De Vittorio, R. Joray, J.X. Chen, R.P. Stanley, A. Fiore, Semicond. Sci. Technol. **19**, 333 (2004)
10. Y.C. Chang, C.S. Wang, L.A. Johansson, L.A. Coldren, Electron. Lett. **42**, 1281 (2006)
11. K.S. Chang, Y.M. Song, Y.T. Lee, Appl. Phys. B, Lasers Opt. **89**, 231 (2007)
12. C.K. Lin, P.D. Dapkus, IEEE Photonics Technol. Lett **13**, 263 (2001)
13. H.C. Yu, S.J. Chang, Y.K. Su, C.P. Sung, H.P. Yang, C.Y. Huang, Y.W. Lin, J.M. Wang, F.I. La, H.C. Kuo, Jpn. J. Appl. Phys. **43**, 1947–1950 (2004)

14. Y.H. Chang, F.I. Lai, C.Y. Lu, H.C. Kuo, H.C. Yu, C.P. Sung, H.P. Yang, S.C. Wang, Semicond. Sci. Technol. **19**, L74 (2004)
15. A.V. Giannopoulos, A.M. Kasten, C.M. Long, C. Chen, K.D. Choquette, Appl. Opt. **47**, 4555 (2008)
16. P. Westbergh, J.S. Gustavsson, A. Haglund, A. Larsson, F. Hopfer, G. Fiol, D. Bimberg, A. Joel, Electron. Lett. **45**, 366 (2009)